ULTRASONIC IMAGING **27,** 237-255 (2005)

Field Computation for Two-Dimensional Array Transducers with Limited Diffraction Array Beams

JIAN-YU LU AND JIQI CHENG

Ultrasound Laboratory
Department of Bioengineering
The University of Toledo
Toledo, OH 43606
jilu@eng.utoledo.edu

A method is developed for calculating fields produced with a two-dimensional (2D) array transducer. This method decomposes an arbitrary 2D aperture weighting function into a set of limited diffraction array beams. Using the analytical expressions of limited diffraction beams, arbitrary continuous wave (cw) or pulse wave (pw) fields of 2D arrays can be obtained with a simple superposition of these beams. In addition, this method can be simplified and applied to a 1D array transducer of a finite or infinite elevation height. For beams produced with axially symmetric aperture weighting functions, this method can be reduced to the Fourier-Bessel method studied previously where an annular array transducer can be used. The advantage of the method is that it is accurate and computationally efficient, especially in regions that are not far from the surface of the transducer (near field), where it is important for medical imaging.

Both computer simulations and a synthetic array experiment are carried out to verify the method. Results (Bessel beam, focused Gaussian beam, X wave and asymmetric array beams) show that the method is accurate as compared to that using the Rayleigh-Sommerfeld diffraction formula and agrees well with the experiment.

Key words: Fourier-Bessel method; limited diffraction array beams; Rayleigh-Sommerfeld diffraction formula; two-dimensional array transducers; ultrasound beams; ultrasound field computations.

I. INTRODUCTION

Transducers are an essential part of medical ultrasound imaging systems.[1] In earlier systems, transducers usually had a single element focused with a lens and images were formed by steering the beams mechanically.[2] Mechanical scanning is slow and the transducer positioning system is bulky and is subject to mechanical wear. In modern imaging systems, electronic focusing and scanning have replaced mechanical scanning in commercial systems except at high frequencies.[2] To steer and focus beams electronically, one-dimensional (1D) array transducers are used. Commercial 1D array transducers typically have 128, 192 or 256 independent elements. Although 1D array transducers can steer and focus beams electronically in a plane defined by the array elements and its axial axis, they are not able to steer beams or change focal distance dynamically perpendicular to this plane (elevation direction). To address this problem, one-and-a-half dimensional (1.5D) or one-and-three-quarter dimensional (1.75D) array transducers were developed.[3,4] The idea is to subdivide the length of each 1D array element into a few subelements to gain some control of beams in the elevation direction to improve image quality without significantly increasing the number of inde-

0161-7346/06 $18.00

pendently-addressable elements (keeping the relative simplicity of the electronics that handle the signals of transducers). Because the width of elements in the elevation direction in 1.5D or 1.75D array transducers is not small enough, it is difficult to steer the beams without causing significant grating lobes in this direction. To be fully flexible in steering and focusing beams in both dimensions for three-dimensional (3D) imaging, fully populated two-dimensional (2D) array transducers were developed.[5, 6] 2D array transducers are also useful in applications such as phase aberration correction,[7, 8] production of limited diffraction beams,[9] and high frame rate (HFR) 3D imaging.[10-16] Therefore, field computations for 2D array transducers are crucial in these applications.

Limited diffraction beams were first studied by Stratton[17] and later by Durnin et al.[18, 19] In 1991, new families of limited diffraction beams called X waves were discovered.[20-22] Based on X waves, limited diffraction array beams[23-25] and the high frame rate 2D and 3D imaging methods have been developed.[10-16] Recently, X waves have been applied to nonlinear optics.[26-34] Theoretically, limited diffraction beams can propagate to an infinite distance without spreading. In practice, when these beams are produced with finite energy and aperture, they have a large depth of field. This property is useful in many applications.[35]

In this paper, a method is developed to calculate the fields produced by 2D array transducers.[36] In this method, the aperture weighting function of a 2D array transducer is decomposed into limited diffraction array beams of different parameters.[23-25] Because limited diffraction beams are propagation invariant, they have simple analytical expressions and thus the total field of a transducer can be obtained by a direct linear superposition of these beams. In addition, this method can be simplified and applied to a 1D array transducer of a finite or infinite elevation height. For beams produced with axially symmetric aperture weighting functions, this method can be reduced to the Fourier-Bessel method studied previously where an annular array transducer can be used.[37-39] The advantage of the method is that it is accurate and computationally efficient, especially in regions that are not far from the surface of the transducer (near field), where it is important for medical imaging.

To verify the method, both computer simulations and a synthetic array experiment[40] are carried out to produce Bessel beams, focused Gaussian beams, X waves and asymmetric array beams using 2D array transducers. Results show that the method is accurate as compared to that using the Rayleigh-Sommerfeld (RS)[41] diffraction formula and agrees well with the experiment.

The method above is different from the approach using the traditional RS diffraction formula,[41] which is based on the Huygens' principle and requires a double integration to calculate wave fields. Although the RS method is accurate, the double integration is time consuming in numerical implementation and is very difficult to calculate fields that are resulted from a rapid change of phase of the integrand (this happens when fields are near the surface and/or off the axial axis of the transducer). Although Fresnel and Fraunhofer approximations to the RS formula may be used to reduce computation in some cases, they are limited to paraxial or far field applications.[41]

Compared to the spatial impulse response methods,[42-46] the method with limited diffraction array beams has advantages. Firstly, the coefficients of different limited-diffraction array beams for a given 2D array transducer and its aperture weighting function can be calculated separately and stored. These coefficients can then be used to compute fields at any point in space by a simple 2D linear superposition. Secondly, the method can take advantage of finite bandwidth of any practical systems to reduce computations. Thirdly, the method does not have the problem of requiring an extremely high sampling rate to calculate the impulse responses that may exhibit Dirac-Delta function characteristics. If the Nyquist sampling rate is not met, impulse response methods may often produce significant artifacts, leading to a misinterpretation of a pulse or image simulated. Finally, impulse response methods require a complicated geometrical operation to calculate the impulse response of each transducer el-

ement and then summed them over all elements. A numerical convolution is also needed to obtain the final wave pulse for each point in space, which can also be time consuming at a high sampling rate.

Another method is the angular spectrum decomposition.[41] This method may be computationally efficient since a 2D fast Fourier transform (FFT) can be used. However, when the FFT is used, the field points in transverse space are predetermined on a rectangular grid. To obtain a field at an arbitrary point in space, either interpolation or a high spatial sampling rate is required. In addition, all field points at a given axial distance in space are calculated even if only one or a few points in space are of interest at that depth, wasting the computation time. If the aperture weighting function contains abrupt changes such as sudden pressure drop to zero at the kerfs of a 2D array transducer, a high sampling rate over the 2D aperture may be required to avoid aliasing.

II. THEORY

In the following, formulas for calculating waves produced by 2D array transducers are developed. The formulas can also be simplified for 1D or annular array transducers. The isotropic/homogeneous wave equation is given by:[47]

$$^2 \quad \frac{1}{c^2}\frac{^2}{t^2} \quad (\vec{r},t) \quad 0 \tag{1}$$

where ^{2} is the Laplace, $(\vec{r},t)$ is the acoustic pressure, velocity potential or Hertz potential in free space, $\vec{r} \quad (x, y, z)$ is a point in the space, t is the time and c is the speed of sound in a medium or the speed of light in vacuum.

Using the Fourier transform relationship, a solution to the wave equation can be expressed as:

$$(\vec{r},t) \quad \frac{1}{2} \quad ^{\sim}(\vec{r}; \quad) e^{\ i\ t} d \tag{2}$$

where $^{\sim}(\vec{r}; \quad)$ is the Fourier transform of $(\vec{r},t)$ in terms of time and $=2\ f$ is the angular frequency, where f is the frequency.

Limited diffraction beams such as X waves are solutions to Eq. (1).[20-22] These solutions do not diffract in theory, meaning that once they are produced, they are able to propagate to an infinite distance without changing their pulse shape in both space and time. With a linear superposition of these beams of different orders, one obtains the following limited diffraction array beam (see the derivations in references 10, 23-25), which is also a solution to Eq. (1):

$$\begin{aligned} ^{uv}_{Array}(\vec{r},t) \quad ^{uv}_{Array}(x,y,z \quad c_1 t) \quad & \frac{1}{2}\int_0 A(k) D_{u,v}(\quad) e^{ik_{x_u}x} e^{ik_{y_v}y} e^{ik_{z_{uv}}z} e^{\ i\ t} dk \\ & \frac{1}{2} \quad A(k)H(k)D_{u,v}(\quad) e^{i\vec{K}_{uv}\ \vec{r}\ \ i\ t} dk \end{aligned} \tag{3}$$

where the subscript 'Array' means array beam, u and v are integers, $k= \ /c$ is the wave number, $A(k)$ is the electromechanical transfer function of a transducer, $D_{u,v}(\ )$ are complex coef-

ficients, $c_1=c/\cos$ is the wave speed, where is the Axicon angle[10] of the X waves ($k_{x_u}=k\sin\cos$, $k_{y_v}=k\sin\sin$ and $k_{z_{uv}}=k\cos$, where - (or 0) is a free parameter or the azimuthal angle) and $H(k)$ is the Heaviside step function:[48]

$$H(\frac{}{c}) \quad \begin{matrix} 1, & 0 \\ 0, & 0 \end{matrix} \tag{4}$$

$\vec{K}_{uv}$ $(k_{x_u}, k_{y_v}, k_{z_{uv}})$ is the wave vector and where

$$k_{z_{uv}} \quad \sqrt{k^2 \quad k_{x_u}^2 \quad k_{y_v}^2} \tag{5}$$

From Eq. (3), one obtains the spectrum of $_{Array}^{uv}(\vec{r},t)$:

$$\sim_{Array}^{uv}(\vec{r}; \ ) \quad \frac{A(k)H(k)}{c} D_{u,v}(\ ) e^{i\vec{K}_{uv}\ \vec{r}} \tag{6}$$

If the system is assumed linear, the total field at $\vec{r}$ is a linear superposition of those produced by Eq. (6) (assuming that the summation exists):

$$\sim(\vec{r}, \ ) \qquad \frac{A(k)H(k)}{c} D_{u,v}(\ ) e^{i\vec{K}_{uv}\ \vec{r}} \tag{7}$$
$$u \quad v$$

Now, let us determine the coefficients $D_{u,v}(\ )$, for a 2D array of a given aperture weighting function. Assuming that a planar 2D array transducer is located at the plane $z=0$, the field produced at the transducer surface is given by:

$$\sim(\vec{r}_1; \ ) \qquad \begin{matrix} \tilde{Q}(\vec{r}_1; \ ), & (|x_1| \quad w_x, \ |y_1| \quad w_y) \\ 0, & (w_x \quad |x_1| \quad R_x, \ w_y \quad |y_1| \quad R_y) \end{matrix} \tag{8}$$

where $\tilde{Q}(\vec{r}_1; \ )$ is the field at the surface of the transducer, $\vec{r}_1$ $(x_1, y_1, 0)$ is a point at the surface and w_x and w_y are the half widths of the aperture size of the array transducer along the x_1 and y_1 axes, respectively (Fig. 1). The array transducer is assumed to be surrounded by a rectangular frame ($w_x<|x_1| \ R_x$, $w_y<|y_1| \ R_y$) with zero field amplitude, where R_x and R_y are the half widths of the outer frame. In addition, the pattern in Eq. (8) is periodically repeated outside of the frame bounded by ($|x_1| \ R_x$, $|y_1| \ R_y$) with periods of $2R_x$ and $2R_y$ in the x_1 and y_1 directions, respectively. Apparently, as both R_x and R_y , Eq. (8) represents a single array without a spatial repetition.

Since Eq. (8) is a periodic function, it can be expanded as a Fourier series[48] with periods of $2R_x$ and $2R_y$ along the x_1 and y_1 axes, respectively. Letting $z=0$ in Eq. (7), we obtain such a series:

$$\sim(\vec{r}_1; \ ) \qquad \frac{A(k)H(k)}{c} D_{u,v}(\ ) e^{ik_{x_u}x_1} e^{ik_{y_v}y_1} \tag{9}$$
$$u \quad v$$

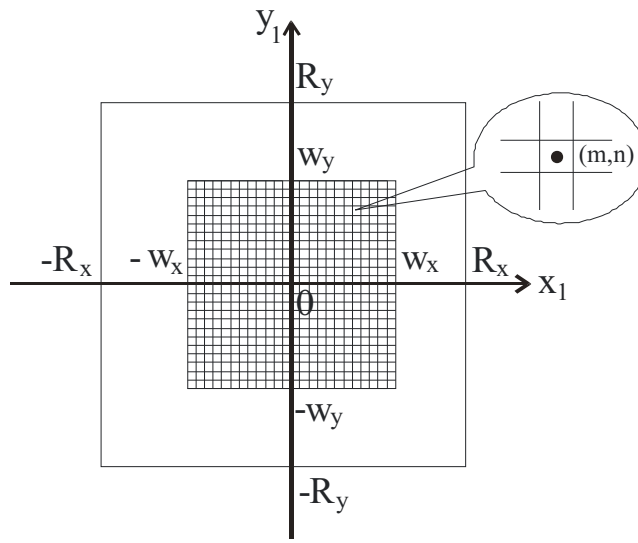

FIG. 1 Coordinates of a 2D array transducer.

where

$$k_{x_u} \quad \frac{u}{R_x} \tag{10}$$

and

$$k_{y_v} \quad \frac{v}{R_y} \tag{11}$$

and where $u,v = 1, \quad 2, \quad 3,$

The coefficients of the Fourier series in Eq. (9) are given by:[48]

$$\frac{A(k)H(k)}{c} D_{u,v}(\quad) \quad \frac{1}{4R_xR_y} \int_{w_x}^{w_x} \int_{w_y}^{w_y} \tilde{}(\vec{r}_{1;} \quad) e^{\ ik_{x_u}x_1} e^{\ ik_{y_v}y_1} dx_1 dy_1 \tag{12}$$

Assuming that an array transducer consists of $M \quad N$ rectangular elements and the spatially quantized driving and aperture weighting function of an element centered at (x_{1_m}, y_{1_n}) is $\tilde{}_{m,n}(\quad) \quad \tilde{}(x_{1_m}, y_{1_n}; \quad)$, where $1 \quad m \quad M, 1 \quad n \quad N$, and M and N are integers, the integration in Eq. (12) can be precalculated and stored as known coefficients:

(13)

$$\begin{aligned}
\frac{A(k)H(k)}{c} D_{u,v}(\quad) \quad & \frac{1}{4R_xR_yk_{x_u}k_{y_v}} \sum_{m\ 1}^{M} \sum_{n\ 1}^{N} \tilde{}_{m,n}(\quad)(e^{ik_{x_u}w_{x_m}} \quad e^{\ ik_{x_u}w_{x_m}})(e^{ik_{y_v}w_{y_n}} \quad e^{\ ik_{y_v}w_{y_n}}) e^{\ ik_{x_u}x_{1_m}\ ik_{y_v}y_{1_n}} \\
& \frac{1}{R_xR_yk_{x_u}k_{y_v}} \sum_{m\ 1}^{M} \sum_{n\ 1}^{N} \tilde{}_{m,n}(\quad)\sin(k_{x_u}w_{x_m})\sin(k_{y_v}w_{y_n}) e^{\ ik_{x_u}x_{1_m}\ ik_{y_v}y_{1_n}} \\
& \frac{1}{R_xR_y} \sum_{m\ 1}^{M} \sum_{n\ 1}^{N} w_{x_m}w_{y_n} \tilde{}_{m,n}(\quad)\mathrm{sinc}(k_{x_u}w_{x_m})\mathrm{sinc}(k_{y_v}w_{y_n}) e^{\ ik_{x_u}x_{1_m}\ ik_{y_v}y_{1_n}}
\end{aligned}$$

where w_{x_m} and w_{y_n} are the half widths of the transducer element centered at (x_{1_m}, y_{1_n}) along the x_1 and y_1 axes, respectively, and sinc( ) is the sinc function. If $\tilde{}_{m,n}(\ ) \quad E(\ )G(x_{1_m}, y_{1_n})$, where $E(\ )$ is the spectrum of the excitation signal of the transducer and $G(x_{1_m}, y_{1_n})$ is a transducer aperture weighting function that is not a function of , the double summation in Eq. (13) needs to be calculated only once and then stored for all , saving computer memory usage and speeding up the computation. For a 1D array transducer (N=1) with a finite elevation width (y_1 direction), the double summation in Eq. (13) is reduced to a single summation. If the height of the 1D array in elevation is infinity, then k_{y_v} and thus the field will not be a function of y. In this case, it is easy to obtain a 1D version of Eq. (13):

$$\frac{A(k)H(k)}{c} D_u(\ ) \quad \frac{1}{R_x} \sum_{m\ 1}^{M} w_{x_m} \tilde{}_m(\ )\,\mathrm{sinc}(k_{x_u} w_{x_m}) e^{\ ik_{x_u} x_{1_m}} \tag{14}$$

It is seen that both the indices v and n in Eq. (14) are removed, greatly simplifying the computation.

From Eqs. (7) and (2), one obtains the wave produced by a 2D array (it is clear that this formula as well as Eq. (7) show that limited diffraction beams are very useful in forming analytically an arbitrary physical beam):

$$(\vec{r},t) \quad \frac{1}{2} \quad \frac{A(k)H(k)}{c} \qquad \sum_{u \quad v} D_{u,v}(\ ) e^{i\vec{K}_{uv}\ \vec{r}} \ e^{\ i\ t} d \tag{15}$$

where the coefficient, $A(k)H(k)D_{u,v}(\ )/c$, is given by Eq. (13). For a single array transducer without repeating over the plane, z=0, the Fourier series in Eq. (15) can be evaluated with Fourier integrals through the following limits:[48]

$$(\vec{r},t) \quad \lim_{R_x,R_y} \quad \frac{1}{2} \quad \frac{A(k)H(k)}{c} \qquad \sum_{u \quad v} D_{u,v}(\ ) e^{i\vec{K}_{uv}\ \vec{r}} \ e^{\ i\ t} d \tag{16}$$

In ultrasonic imaging, the region of interest is usually in the near field and around the axial axis of a transducer. In this case, both R_x and R_y need only to be a few times bigger than the corresponding dimensions of the transducer to obtain accurate results. This can be seen from the computer simulations in the next section.

The infinite sums in both Eqs. (15) and (16) are not necessary because as $|u|$ and $|v|$ increase, $k_{x_u}^2 \quad k_{yv}^2$ will exceed k^2 and this makes $k_{z_{uv}}$ in Eq. (5) imaginary. For imaginary $k_{z_{uv}}$, the corresponding components in Eqs. (15) and (16) become evanescent waves that attenuate rapidly along the z axis (usually within a few wavelengths). Let k_{x_u} change from *–k to k;* according to Eq. (10), u will then change from $-u_{\max}(k)$ to $u_{\max}(k)$, where $u_{\max}(k)$ is an integer that is larger than but is the closest to $kR_x/\ $, or,

$$u_{\max}(k) \quad \frac{kR_x}{} \quad \frac{2R_x}{} \tag{17}$$

From Eqs. (5) and (11), the change of v is allowed to be from $-v_{\max}(u,k)$ to $v_{\max}(u,k)$, where $v_{\max}(u,k)$ is an integer that is larger than but is the closest to $R_y\sqrt{k^2 \quad (u\ /R_x)^2}\ /\ \ $. Using these conditions, Eq. (15) can be written as:

$$(\vec{r},t) \quad \frac{1}{2} \quad \frac{A(k)H(k)}{c} \quad \sum_{u \quad u_{\max}(k)}^{u_{\max}(k)} \sum_{v \quad v_{\max}(u,k)}^{v_{\max}(u,k)} D_{u,v}(\quad) e^{i\vec{K}_{uv}\vec{r}} \quad e^{i \quad t} d \tag{18}$$

The Fourier transform in terms of time in Eq. (18) can be calculated with the discrete Fourier transform (DFT) or fast Fourier transform (FFT).[49] Corresponding to Eq. (14), Eq. (18) can be simplified for a 1D array of an infinite height in elevation direction:

$$(\vec{r},t) \quad \frac{1}{2} \quad \frac{A(k)H(k)}{c} \quad \sum_{u \quad u_{\max}(k)}^{u_{\max}(k)} D_u(\quad) e^{i\vec{K}_u\vec{r}} \quad e^{i \quad t} d \tag{19}$$

where $\vec{r} \quad (x,z)$, $\vec{K}_u \quad (k_{x_u}, k_{z_u})$ and where $k_{z_u} \quad \sqrt{k^2 \quad k_{x_u}^2}$.

In a practical ultrasonic imaging system, *A(k)* in Eqs. (18) and (19) is a bandpass function and can be approximately modeled as a Blackman window function:[50]

$$A(k) \quad \begin{array}{ll} 0.42 \quad 0.5\cos\dfrac{k}{k_c} \quad 0.08\cos\dfrac{2 \quad k}{k_c}, & 0 \quad k \quad 2k_c \\ 0 & \text{Otherwise} \end{array} \tag{20}$$

where $k_c=2 \quad f_c/c$ and f_c is the center frequency. Thus the 6dB bandwidth of *A(k)* is about 81% of its center frequency, which is typical for medical ultrasound. Due to the bandlimited nature, the computation for Eqs. (18) and (19) can be further reduced (fewer discrete are needed).

It is worth noting that if the aperture-weighting function is axially symmetric, the limited diffraction array beam method for 2D array transducers can be simplified to the Fourier-Bessel method studied previously where an annular array transducer can be used.[37-39] The limited diffraction array beam $\tilde{}^{uv}_{Array}(\vec{r}, \quad)$, in Eq. (6) can be used to construct other axially symmetric limited diffraction beams that are a function of a radial distance $r \quad \sqrt{x^2 \quad y^2}$ but are not a function of the azimuthal angle, - $< \quad$. Assuming that $k_{x_u} \quad {}_u \cos \quad$ and $k_{y_v} \quad {}_u \sin \quad$, where ${}_u$ and are free parameters, from Eq. (5), one obtains $k_{z_{uv}} \quad {}_u \quad \sqrt{k^2 \quad {}^2_u}$. Inserting k_{x_u}, k_{y_v} and $k_{z_{uv}}$ into Eq. (6) and averaging the result for from 0 to 2, one obtains the spectrum of a limited diffraction Bessel beam[18-19, 21] that is a solution to the wave equation Eq. (1):

$$\begin{aligned} \tilde{}^{u}(r,z; \quad) \quad & \frac{A(k)H(k)}{c} D_{u,v}(\quad) \quad \frac{1}{2} \quad e^{i\vec{K}_{uv}\vec{r}} d \\ & \frac{A(k)H(k)}{c} D_u(\quad) J_0(\quad {}_u r) e^{i \quad {}_u z} \end{aligned} \tag{21}$$

where u=1,2,3, .,.and $J_0(\quad {}_u r)$ is the zeroth-order Bessel function of the first kind. Similar to Eq. (7), a linear superposition of Eq. (21) is still a solution to the wave equation at a single frequency (assuming that the summation exists):

$$\tilde{} \quad r,z; \quad) \quad \frac{A(k)H(k)}{c} \quad \sum_{u \quad 1} D_u(\quad) J_0(\quad {}_u r) e^{i \quad {}_u z} \tag{22}$$

Similar to Eq. (9), any well-behaved axially symmetric aperture weighting function at the transducer surface (z=0) can be expressed as a Fourier-Bessel series[48] over the integer, u, with $_u=q_u/R$, where q_u is the uth root of $J_0(\ )$ (i.e., $J_0(q_u)\ \ 0$) and $R\ \ a$ is the outer radius of the aperture-weighting function of the transducer, and where a is the radius of the weighting function (the weighting function is assumed to be zero for $a\ \ r_1\ \ R$, where $r_1\ \ \sqrt{x_1^2\ \ y_1^2}$):

$$\tilde{}(r_1;\ \ )\ \ \frac{A(k)H(k)}{c}\ \ _{u\ 1} D_u(\ \ )J_0(\ \ _u r_1) \tag{23}$$

The coefficient, $D_u(\ \ )$, can be obtained from a formula similar to Eq. (12):[37-39]

$$\frac{A(k)H(k)}{c} D_u(\ \ )\ \ \frac{2}{R^2 J_1^2(q_u)}\ _0^a \tilde{}\ \ r_1;\ \ )J_0(\ \ _u r_1) r_1 dr_1 \tag{24}$$

where $\tilde{}(r_1;\ \ )$ is the field at the surface of the transducer and $J_1(\ )$ is the first-order Bessel function of the first kind. Equations (22) and (24) form the basis of the Fourier-Bessel method.[37-39] They are suitable for calculating fields produced with an annular array transducer. Similar simplification steps leading to Eqs. (13) and (18) are also applicable to Eqs. (24) and (22), respectively.

III. SIMULATION AND EXPERIMENTAL RESULTS

A. Transducer and experimental conditions

For numerical examples in the following subsections, two array transducers are assumed. One has 50 50 equal-sized elements, while the other has 250 250. Both arrays have a total area of 50mm 50mm. For simplicity, kerfs between the elements are not considered. The center frequency of the transducers is assumed to be f_c=2.5MHz. In the pulse-wave (pw) study, a tapered sine wave of about one-and-a-half cycles is used to excite the transducers:

$$e(t)\ \ \begin{array}{ll} e^{\ t^2/t_0^2}\sin(2\ \ f_c t), & 0\ \ t\ \ 20.48\mu s \\ 0 & \text{Otherwise} \end{array} \tag{25}$$

where t_0=0.4 s. Taking a Fourier transform of (Eq. 25), we have:

$$E(\ \ )\ \ \ _t\ e(t) \tag{26}$$

where $_t$ represents the the Fourier transform in terms of time.

To verify the simulation results, data from a synthetic array experiment[40] were used to produce various beams. In the experiment, a broadband PZT ceramic/polymer composite transducer of about 1 mm effective diameter and 2.5MHz center frequency was used to scan in a raster format. At the centers of elements of an equivalent 2D array of 50mm wide aperture, the transducer emitted a short pulse. A polyvinylidene fluoride (PVDF) needle hydrophone of 0.5mm diameter was used to receive the waves produced by the transducer at various spa-

tial points. The measured data were then used to form various beams by applying different aperture weightings. More details of the experiment are given in reference 40.

B. Simulation and experiment of cw fields

Three cw fields are studied in this section. The first is a zeroth-order Bessel beam,[18, 19] which has the following aperture weighting function:

$$\sim_{m,n}(\ ) \quad \begin{cases} \dfrac{A(k)H(k)}{c} E(\ ) J_0(\ r_{1_{m,n}}), & r_{1_{m,n}} \quad 25\text{mm} \\ 0, & \text{Otherwise} \end{cases} \tag{27}$$

where =1202.45m^{-1} is a scaling parameter, $r_{1_{m,n}}$ $\sqrt{x_{1_m}^2 \quad y_{1_n}^2}$ is the radius to the center of the element (m,n) from the center of the array transducer and $E(\ )$ is a complex constant at a single frequency. In the case of Bessel beam or any axially symmetric beams, the Fourier-Bessel method using an annular array transducer can be used to reduce the computation.[37-39]

The second is a focused Gaussian beam[51] with the following aperture weighting function:

$$\sim_{m,n}(\ ) \quad \begin{cases} \dfrac{A(k)H(k)}{c} E(\ ) e^{\ r_{1_{m,n}}^2 / \ ^2} e^{\ ik(\sqrt{F^2 \ \ r_{1_{m,n}}^2} \ \ F)}, & r_{1_{m,n}} \quad 25\text{mm} \\ 0, & \text{Otherwise} \end{cases} \tag{28}$$

where =15mm with a corresponding full width at half maximum (FWHM) of 25mm for the Gaussian function and F=100mm is the focal distance of the beam.

The third is an asymmetric array beam, which is defined as:[23-25]

$$\sim_{m,n}(\ ) \quad \begin{cases} \dfrac{A(k)H(k)}{c} E(\ ) \cos k_{x_0} x_{1_m} \cos k_{y_0} y_{1_n}, & r_{1_{m,n}} \quad 25\text{mm} \\ 0, & \text{Otherwise} \end{cases} \tag{29}$$

where k_{x_0} 1,000 m^{-1} and k_{y_0} 500 m^{-1} are scaling factors of the array beam.

The simulations for the first two beams are carried out using both Eqs. (13) and (18) for both 50 50 and 250 250 element arrays. For the third beam, results are obtained for the 250 250 element array only. To reduce the amount of computation in obtaining the coefficients in Eq. (13), we first assume that R_x=2w_x=50 mm and R_y=2w_y=50 mm to calculate the coefficients and denote them $D^*_{u,v}(\ )$. This increases the step size of both k_{x_u} and k_{y_v} according to Eqs. (10) and (11), respectively. To increase the accuracy of the field calculation, we then set R_x=10w_x and R_y=10w_y. The increased number of coefficients $D_{u,v}(\ )$ is obtained with a bilinear interpolation (or other more accurate interpolation scheme such as zero padding) from $D^*_{u,v}(\ )$. Note that the settings, R_x=10w_x and R_y=10w_y, are conservative for the fields simulated in this paper. Larger R_x/w_x and R_y/w_y ratios are only needed when simulated fields are very far from the transducer surface as compared to the physical size of the transducer or are outside of the aperture projection area of the transducer. In general, the farther away a simulated field point is outside of the aperture projection area of a transducer or away from the surface of the transducer, the larger the ratios will be. In medical imaging applications

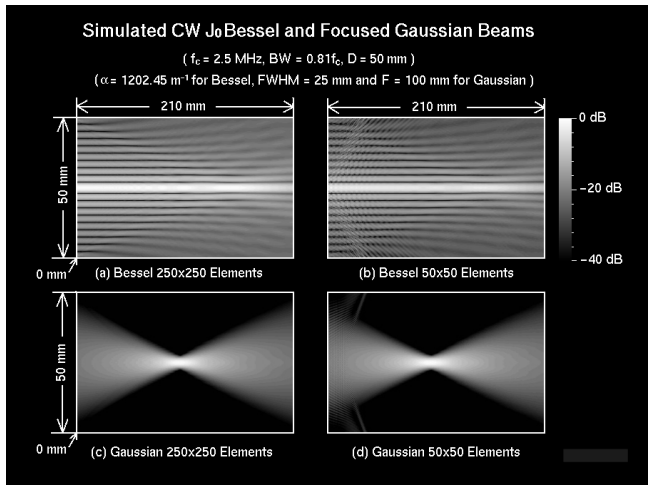

FIG. 2 Cw fields (through the axial axis) simulated with limited diffraction array beams for a Bessel beam ((a) and (b)) and a focused Gaussian beam ((c) and (d)) that are produced with a 2.5 MHz and 50 mm 50 mm 2D array transducer of 250 250 ((a) and (c)) and 50 50 ((b) and (d)) square elements. The horizontal dimensions of the images are along the z axis and the vertical direction is transverse to the beams. Stepwise aperture weightings are assumed for both Bessel and focused Gaussian beams. The scaling parameter for the Bessel weighting is 1202.45 m^{-1}. The focal length and the full-width-at-half-maximum (FWHM) of the focused Gaussian weighting are 100 mm and 25 mm, respectively. The images are log compressed with a dynamic range of 40 dB.

where near fields are of concern, the ratios can be smaller. Further reduction of computation can be achieved by taking advantage of the symmetry of the aperture weighting functions in Eqs. (27) and (28). After getting $D_{u,v}(\ )$, a cw version of Eq. (18) is used to calculate the field (see also Eq. (7)):

$$\tilde{}(\vec{r};\ ) \quad \frac{A(k)H(k)}{c} \sum_{u\ \ u_{\max}(k)}^{u_{\max}(k)} \sum_{v\ \ v_{\max}(u,k)}^{v_{\max}(u,k)} D_{u,v}(\ ) e^{i\vec{K}_{uv}\ \vec{r}} \tag{30}$$

Figure 2 shows the fields simulated with limited diffraction array beam method (using Eqs. (13) and (30)) for both Bessel and focused Gaussian aperture weightings as defined in Eqs. (27) and (28), respectively. Figures 2(a) and 2(c) are produced with an array of 250 250 elements. As a comparison, fields produced with an array of 50 50 elements but with the same array dimension (50 mm 50 mm) are shown in figures 2(b) and 2(d). It is clear that as the number of array elements is reduced while the size of each element increases (less accurate aperture weighting quantization), the influence of the edge waves of the elements appear at distances near the surface of the transducer. After some distance, the influence is negligible. In addition, the Bessel beam has a very large depth of field as compared with the focused Gaussian beam. Figures 3 and 4 show a comparison among the results obtained from the limited diffraction array beam method, the Rayleigh-Sommerfeld diffraction formula, and the synthetic array experiment.[40] The results of the limited diffraction array beam method and the RS method are virtually the same. However, the limited diffraction array beam method allows very accurate and fast computation for fields near the surface of transducers as compared to the RS method. In the RS method, fast phase changes near the surface of the transducers make the convergence of double integration difficult. The results also agree well with those obtained with the synthetic array experiment. Some differences between the simulation and experiment are due to the inaccuracies of the synthetic array ex-

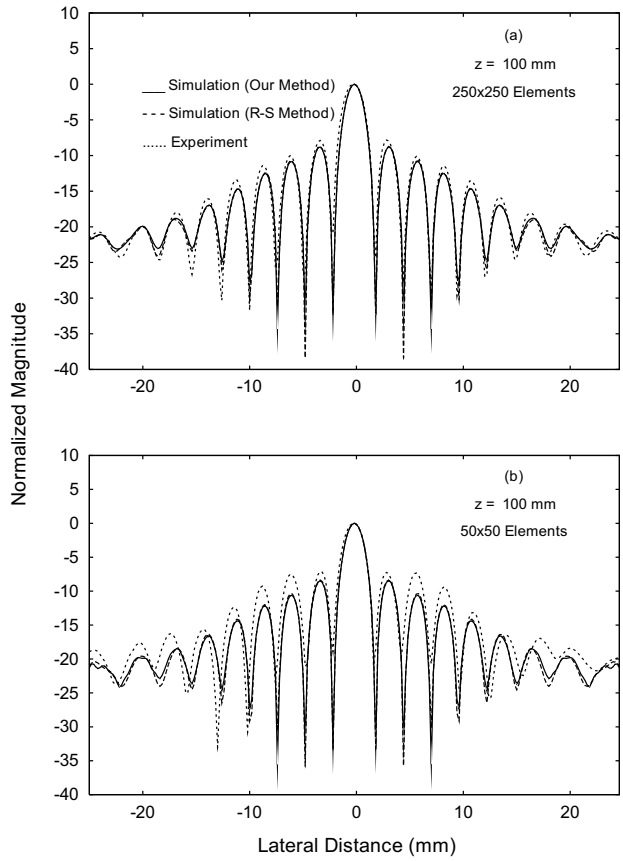

FIG. 3 Lateral line plots of the cw Bessel beams in figure 2 at axial distance $z = 100$ mm away from the surface of the 2D array transducer of (a) 250 250 and (b) 50 50 square elements, respectively. Solid lines represent simulation results with limited diffraction array beams while dashed lines are the results with the Rayleigh-Sommerfeld diffraction formula. Dotted lines are the experiment results obtained with the synthetic array experiment described in reference 40.

periment, such as the size of the point source, positioning inaccuracies in both transverse and axial directions, noise and influence of nonlinear propagation of waves in water.

Let us see an example showing relative computation speed between the method with limited diffraction array beams and the RS method. A cw filed is calculated under the same conditions as those for figure 2(b) except that $R_x = 10w_x$ and $R_y = 10w_y$ are directly used in Eq. (13) to get coefficients without any interpolations. In this case, with a 3.0GHz Intel Pentium 4 computer of 2GB memory and a C program in Linux, it takes about 22 minutes and 19.2 seconds to calculate the coefficients with Eq. (13) and additional 95 minutes and 42 seconds to get the field using Eq. (30). With the RS method, it takes about 108 minutes and 3.6 seconds to calculate only one vertical line at a depth of 100 mm shown in figure 3(b). There are 210 vertical lines in figure 2(b) and each line has 125 points. This means that to obtain the same vertical line, the limited diffraction array beam method requires only about 27.34 seconds if the coefficients are precalculated with Eq. (13). If interpolations are used, the time for getting the coefficients with Eq. (13) can be reduced.

For the asymmetrical array beam weighting in Eq. (29), simulation results are obtained for only one array of 250 250 elements. Unlike the format of figure 2, the asymmetrical beam is shown in the x-y plane (Fig. 5) at several depths. Figure 6 compares the results between the

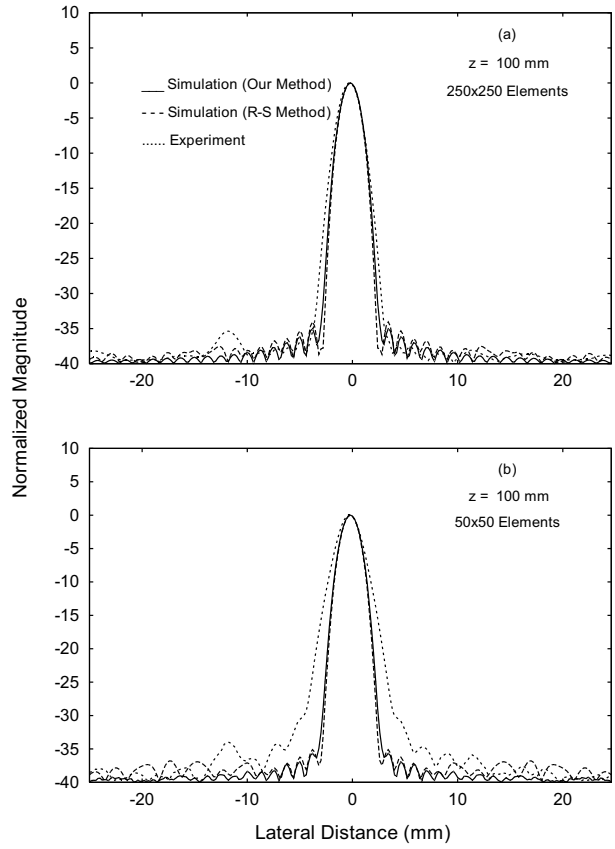

FIG. 4 Same as figure 3, except that it is for the cw focused Gaussian beam. The focal length and the FWHM of the beam are the same as those in figure 2.

limited diffraction array beam method and the synthetic array experiment. The results also agree well with each other.

C. Simulation and experiment for pw fields

Zeroth-order X wave, focused Gaussian pulse and asymmetrical array beam pulse focused in the *x* direction are simulated and verified by the synthetic array experiment in the following pw studies. Similar computation reduction methods for cw fields are also used for pw fields. $R_x=10w_x$ and $R_y=10w_y$ are assumed in the simulation.

For a zeroth-order X wave, the spectrum of the aperture weighting function is given by:

$$\sim_{m,n}(\quad) \quad \begin{cases} \dfrac{2\quad a_0 A(k)H(k)}{c^2} E(\quad) e^{\ a_0 k} J_0(kr_{1_{m,n}} \sin\quad), & r_{1_{m,n}} \quad 25\text{mm} \\ 0, & \text{Otherwise} \end{cases} \tag{31}$$

where a_0=0.05 mm is a parameter that determines the fall-off speed of the high-frequency components of X waves, $=4^0$ is an Axicon angle[52, 53] and c=1,500 m/s is the speed of sound in water.

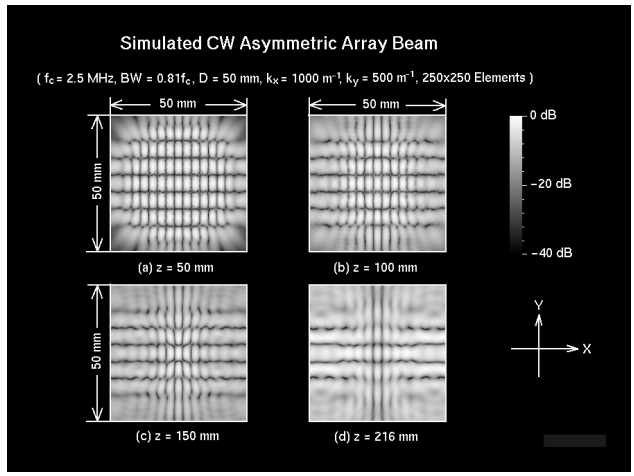

FIG. 5 Transverse cw fields simulated with limited diffraction array beams for an asymmetrical grid array beam[23-25] that is produced with a 2.5 MHz and 50 mm 50 mm 2D array transducer of 250 250 square elements at four axial distances, (a) $z = 50$ mm, (b) $z = 100$ mm, (c) $z = 150$ mm and (d) $z = 216$ mm away from the transducer surface. A stepwise aperture weighting is assumed for the asymmetrical grid array beam. The scaling parameters are 1000 m^{-1} and 500 m^{-1} along the x_1 and y_1 axes, respectively. The images are log compressed with a dynamic range of 40 dB.

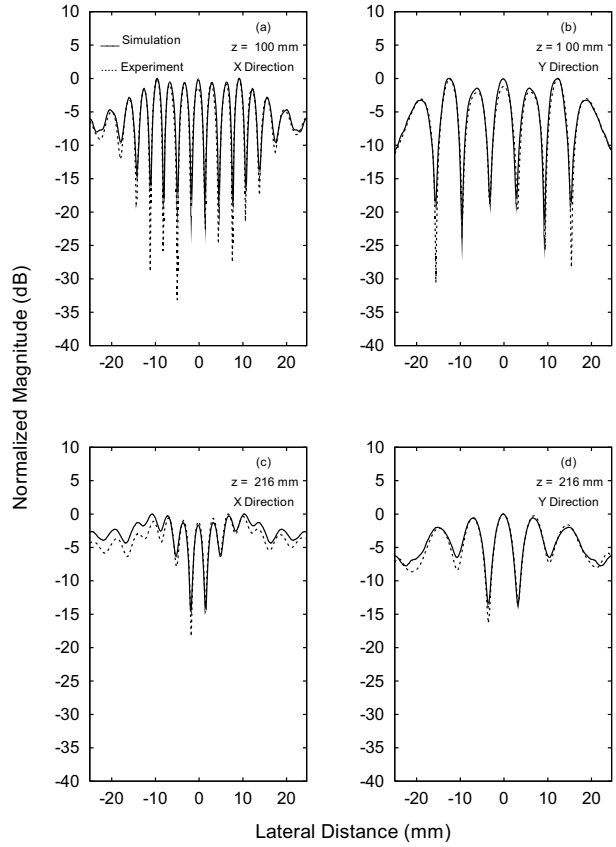

FIG. 6 Lateral line plots of the cw asymmetrical array beam in figure 5 at two axial distances, $z = 100$ mm ((a) and (b)) and $z = 216$ mm ((c) and (d)). At each distance, line plots are given in both the x ((a) and (c)) and y ((b) and (d)) axes. Solid lines represent simulation results with limited diffraction array beams while dotted lines are results with the synthetic array experiment described in reference 40.

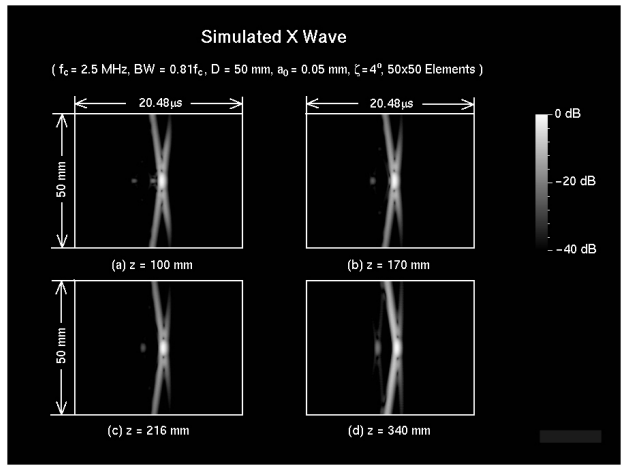

FIG. 7 An X wave (through the axial axis) simulated with limited diffraction array beams and produced with a 2.5 MHz and 50 mm 50 mm 2D array transducer of 50 50 square elements at four axial distances, (a) $z = 100$ mm, (b) $z = 170$ mm, (c) $z = 216$ mm, and (d) $z = 340$ mm, away from the transducer surface. The horizontal direction of the images is the time and the vertical dimension is transverse to the wave axis. A broadband pulse excitation and a stepwise aperture weighting are assumed. The free parameter, a_0, and the Axicon angle, , are assumed to be 0.05 mm and 4 degrees, respectively. The transmitting transfer function of the 2D array is assumed to be a Blackman window function peaked at the center frequency of 2.5 MHz, and the -6dB bandwidth of the array is about 81% of the center frequency. The images have the same dynamic range as those in figure 2.

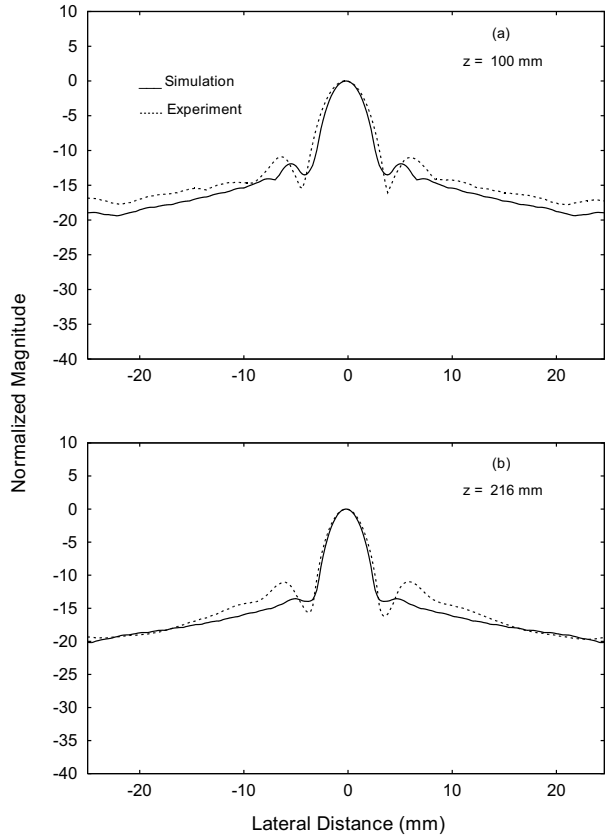

FIG. 8 Lateral plots of the maximum sidelobes of the X wave in figure 7 at two axial distances, (a) $z = 100$ mm and (b) $z = 216$ mm. The plots are transverse to the axial axis of the wave. Solid lines show the simulation results using limited diffraction array beams and the dotted lines are those from the synthetic array experiment.[40]

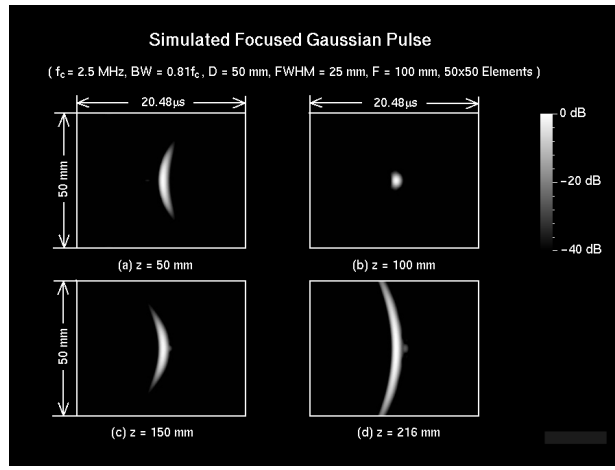

FIG. 9 This figure is the same as figure 7, except that it is a broadband focused Gaussian pulse at four axial distances, (a) $z = 50$ mm, (b) $z = 100$ mm, (c) $z = 150$ mm and (d) $z = 216$ mm away from the transducer surface. The focal length and the FWHM of the pulse are the same as those of the cw focused Gaussian beam in figure 2.

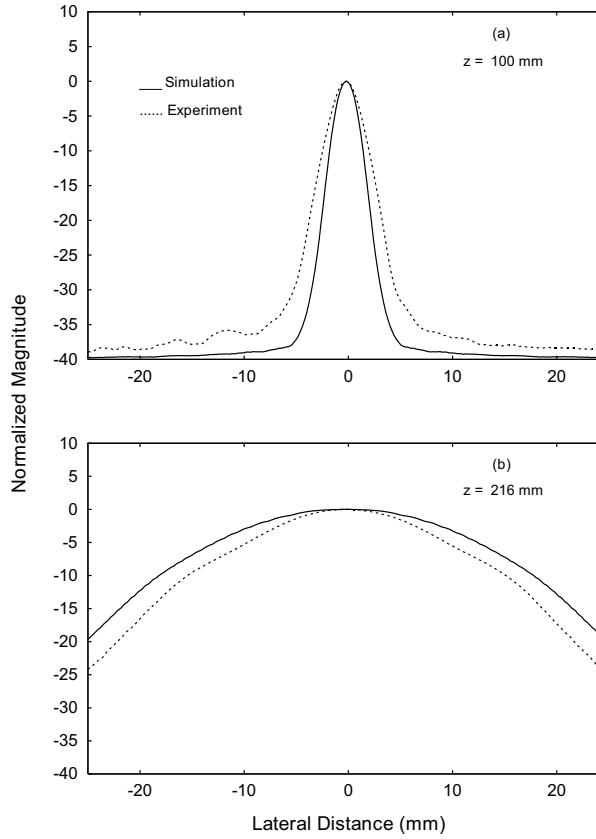

FIG. 10 Same as figure 8, except that it shows the lateral plots of the maximum sidelobes of the focused Gaussian pulse in figure 9 at two axial distances.

For a focused Gaussian pulse, the aperture weighting function is the same as that in Eq. (28).

The aperture weighting function of the asymmetrical array beam focused in the x direction is given by:

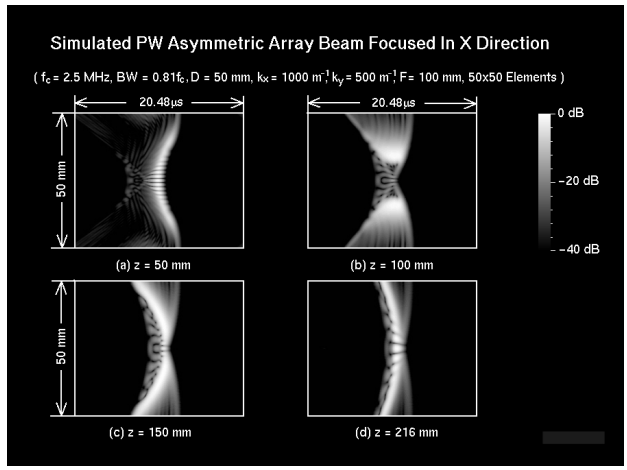

FIG. 11 Same as figure 9, except that it is a broadband focused asymmetrical array beam. Beam profiles in the x-t plane are shown. The scaling parameters in the x_1 and y_1 directions are the same as those of the cw asymmetrical array beam in figure 5. A cylindrical lens of a focal length of 100 mm is added in the x_1 direction.

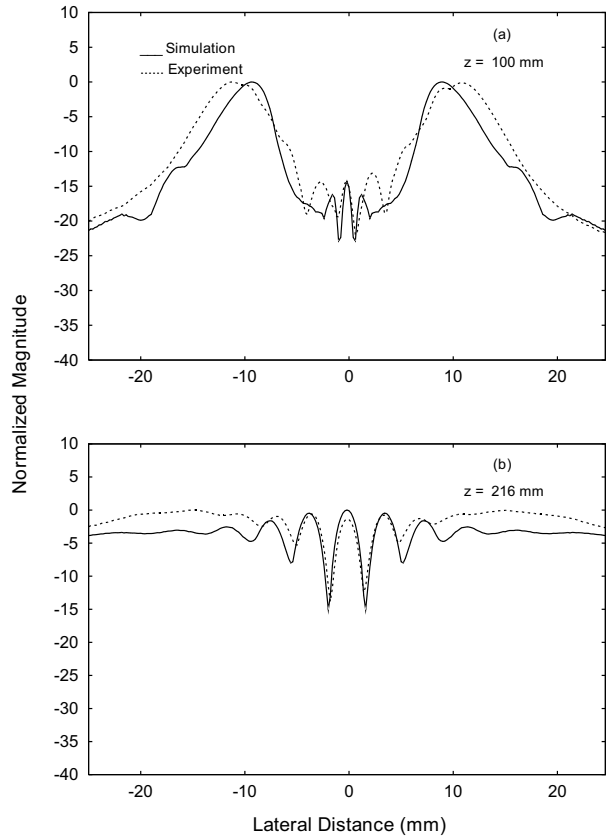

FIG. 12 Same as figure 8, except that it is for the asymmetrical array beam with a lens added in the x_1 direction as shown in figure 11.

$$\sim_{m,n}(\ ) \quad \frac{A(k)H(k)}{c} E(\ ) \cos k_{x_0} x_{1_m} \cos k_{y_0} y_{1_n} e^{\,ik(\sqrt{F^2 \quad x_{1_m}^2} \quad F)}, \quad r_{1_{m,n}} \quad 25\text{mm} \tag{32}$$

$$0, \qquad \text{Otherwise}$$

where F=100 mm is the focal length and other parameters are the same as those in Eq. (29).

After obtaining the coefficients $D_{u,v}(\ )$ with Eq. (13), from the aperture weighting functions Eqs. (28), (31) and (32), pw waves can be calculated with Eq. (18).

Figure 7 shows an X wave simulated with the limited diffraction array beam method (using Eqs. (13) and (18)) at four axial distances using a 50 50 element array transducer. The aperture weighting function is given by Eq. (31). The shape of the letter 'X' is evident in the images. The center spot of the wave keeps its shape over a large traveling distance. The X wave is broadband (has a short temporal duration). Figure 8 shows the maximum sidelobes at two axial distances and compares the results obtained with the limited diffraction array beam method with the synthetic array experiment.[40]

A focused pw Gaussian beam is shown in figure 9 in a similar format as that of figure7. The aperture weighting function is given by Eq. (28) and is the same as that of the cw focused Gaussian beam in figure 2 except that the bandwidth in figure 9 is wide, resulting in a short pulse. Other parameters of the beam are the same as those in figure 2. The maximum sidelobes of the pulse at two axial distances are shown in figure 10 for results from both the simulation and the synthetic array experiment.

Figure 11 shows an asymmetrical array beam pulse focused at 100 mm in the x direction. The pulse is shown in the x-t plane through the axial axis, z, in a similar format as that of figure 9. The Fourier transform characteristic at the focal distance is clearly seen (a donut-hole shape of the pulse). The comparison between the simulation in figure 11 and the results obtained with the synthetic array experiment is shown in figure 12.

IV. CONCLUSION

In this paper, a method to calculate continuous wave (cw) and pulse wave (pw) fields of two-dimensional (2D) array transducers is developed using limited diffraction array beams.[23-25] This method can also be simplified for one-dimensional (1D) array transducers. When the method is applied to axially symmetric beams, where annular array transducers are used, it can be reduced to the Fourier-Bessel method studied previously.[37-39]

Computer simulations and a synthetic array experiment show that the method is accurate and fast as compared to the conventional Rayleigh-Sommerfeld diffraction formula.[41] However, as can be seen from the derivation of the theory, this method is only valid for applications where linearity of wave propagation can be assumed.

ACKNOWLEDGEMENT

This work was supported in part by grant HL60301 from the National Institute of Health.

REFERENCES

1. Von Ramn OT. 2-D arrays, *Ultrasound Med Biology 26* (*Suppl.1*), S10-S12 (2000).

2. Eggleton RC. Johnston KW. Real time mechanical scanning system compared with array techniques, in *1974 IEEE Ultrasonics Symp Proc,* pp. 16-18, (IEEE Catalog no. 74 CHO 896-1SU, 1974).

3. Wildes DG, Chiao RY, Daft CMW, et al. Elevation performance of 1.25D and 1.5D transducer arrays, *IEEE Trans Ultrason Ferroelec Freq Contr 44,* 1027-1037 (1997).

4. Fernandez AT, Keen CG, Gammelmark KL, et al. Adaptive imaging using an 8 X 128 array, in *2000 IEEE Ultrasonics Symp Proc*, vol. 2, pp. 1659-1664 (IEEE Catalog no. 00CH37121, 2000).

5. Greenstein M, Lum P, Yoshida H, Seyed-Bolorforosh MS. A 2.5 MHz 2D array with z-axis backing, in *1996 IEEE Ultrasonics Symp Proc,* vol. 2, pp. 1513-1516 (IEEE Catalog no. 96CH35993, 1996).

6. Davidsen RE, Smith SW. Two-dimensional arrays for medical ultrasound using multilayer flexible circuit interconnection, *IEEE Trans Ultrason Ferroelec Freq Contr 45*, 338-348 (1998).

7. Miwa Y, Shinomura R. Two-directional phase aberration correction using a two-dimensional array, in *1997 IIEEE Ultrasonics Symp Proc*, vol. 2, pp. 1733-1736 (IEEE Catalog no. 97CH36118, 1997).

8. Walker WF, Trahey GE. A fundamental limit on the performance of phase aberration correction and correlation based flow estimates in medical ultrasound, in *1993 IEEE Ultrasonics Symp Proc*, vol. 2, pp. 1149-1153 (IEEE Catalog no. 93CH3301-9, 1993).

9 Lu JY, Greenleaf JF. A study of two-dimensional array transducers for limited diffraction beams, *IEEE Trans Ultrason Ferroelec Freq Contr 41,* 724-739 (1994).

10. Lu JY. 2D and 3D high frame rate imaging with limited diffraction beams, *IEEE Trans Ultrason Ferroelec Freq Contr 44,* 839-856 (1997).

11. Lu JY. Experimental study of high frame rate imaging with limited diffraction beams, *IEEE Trans Ultrason Ferroelec Freq Contr 45,* 84-97 (1998).

12. Cheng J, Lu JY. Extended high frame rate imaging method with limited diffraction beams, *IEEE Trans Ultrason Ferroelec Freq Contr* (May, 2006, in press).

13. Cheng J, Lu JY. Fourier based imaging method with steered plane waves and limited-diffraction array beams, in *2005 IEEE Ultrasonics Symp Proc,* vol. 2, pp. 1976-1979 (IEEE Catalog no. 05CH37716C 2005) (ISSN: 1051-0117).

14. Wang J, Lu JY. A study of motion artifacts of Fourier-based image construction, in *2005 IEEE Ultrasonics Symp Proc*, vol. 2, pp. 1439-1442 (IEEE Catalog no. 05CH37716C, 2005) (ISSN: 1051-0117).

15. Lu JY, Cheng J, Wang J. High frame rate imaging system for limited diffraction array beam imaging with square-wave aperture weightings*, IEEE Trans Ultrason Ferroelec Freq Contr* (submitted).

16. Wade G. Human uses of ultrasound: ancient and modern, *Ultrasonics* 38, 1-5 (2000).

17. Stratton JA. *Electromagnetic Theory,* p. 356 (New York and London: McGraw-Hill Book Company, 1941).

18. Durnin J. Exact solutions for nondiffracting beams. I. The scalar theory, *J Opt Soc Amer A4,* 651–654 (1987).

19. Durnin J, Miceli JJ, Jr., Eberly JH. Diffraction-free beams, *Phys Rev Lett 58,* 1499–1501 (1987).

20. Lu JY, Greenleaf JF. Theory and acoustic experiments of nondiffracting X waves, in *1991 IEEE Ultrasonics Symp Proc*, vol. 2, pp. 1155-1159 (IEEE Catalog no. 91CH3079-1, 1991) (ISSN: 1051-0117).

21. Lu JY, Greenleaf JF. Nondiffracting X waves – exact solutions to free-space scalar wave equation and their finite aperture realizations, *IEEE Trans Ultrason Ferroelec Freq Contr 39,* 19-31 (1992).

22. Lu JY, Greenleaf JF. Experimental verification of nondiffracting X waves, *IEEE Trans Ultrason Ferroelec Freq Contr 39,* 441-446 (1992).

23. Lu JY. Limited diffraction array beams, *Internat J Imag System Tech 8,* 126-136 (1997) (ISSN: 0899-9457).

24. Lu JY. Improving accuracy of transverse velocity measurement with a new limited diffraction beam, in *1996 IEEE Ultrasonics Symp Proc*, vol. 2,p p. 1255-1260 (IEEE Catalog no. 96CH35993, 1996) (ISSN: 1051-0117).

25. Lu JY. Transmit-receive dynamic focusing with limited diffraction beams, in *1997 IEEE Ultrasonics Symp Proc*, vol. 2, pp. 1543-1546 (IEEE Catalog no. 97CH36118, 1997) (ISSN: 1051-0117).

26. Porras MA, Parola A, Faccio D, Dubietis A, Trapani PD. Nonlinear unbalanced Bessel beams: stationary conical waves supported by nonlinear losses, *Phys Rev Lett 93,* 153902 (2004).

27. Kolesik M, Wright EM, Moloney JV. Dynamic nonlinear X waves for femtosecond pulse propagation in water, *Phys Rev Lett 92,* 253901 (2004).

28. Conti C, Trillo S. Nonspreading wave packets in three dimensions formed by an ultracold Bose gas in an optical lattice, *Phys Rev Lett 92,* 120404 (2004).

29. Trapani PD, Valiulis G, Piskarskas A, et al. Spontaneously generated x-shaped light bullets, *Phys Rev Lett 91,* 093904 (2003).

30. Conti C, Trillo S, Trapani PD, et al. Nonlinear electromagnetic X waves, *Phys Rev Lett 90,* 170406 (2003).

31. Salo J, Fagerholm J, Friberg AT, Salomaa MM. Nondiffracting bulk-acoustic X waves in crystals, *Phys Rev Lett 83,* 1171–1174 (1999).

32. Saari P, Reivelt K. Evidence of X-shaped propagation-invariant localized light waves, *Phys Rev Lett 79,* 4135–4138 (1997).

33. Wulle T, Herminghaus S. Nonlinear optics of Bessel beams, *Phys Rev Lett 70,* 1401–1404 (1993).

34. Day C. Intense X-shaped pulses of light propagate without spreading in water and other dispersive media, *Phys Today 57,* 25-26 (2004).

35. Lu JY, Zou H, Greenleaf JF. Biomedical ultrasound beam forming, *Ultrasound Med Biol 20,* 403-428 (1994).

36. Lu JY, Cheng J. Efficient computation of field of 2D array with limited diffraction array beams, *J Acoust Soc Amer 109,* 2397-2398 (2001) (abstract).

37. Fox PD, Cheng J, Lu JY. Fourier-Bessel field calculation and tuning of a cw annular array, *IEEE Trans Ultrason Ferroelec Freq Contr 49,* 1179-1190 (2002).

38. Fox PD, Cheng J, Lu JY. Theory and experiment of Fourier-Bessel field calculation and tuning of a pw annular array, *J Acoust Soc Amer 113,* 2412-2423 (2003).

39. Fox PD, Lu JY, Holm S, Tranquart F. Connection between X waves, Fourier-Bessel series and optimal modeling aperture for circular symmetric arrays, in *2005 IEEE Ultrason Symp Proc*, vol. 2, pp. 1644-1647 (IEEE Catalog no. 05CH37716C, 2005) (ISSN: 1051-0117).

40. Lu JY. Producing bowtie limited diffraction beams with synthetic array experiment, *IEEE Trans Ultrason Ferroelec Freq Contr 43,* 893-900 (1996).

41. Goodman JW. *Introduction to Fourier Optics* (New York, N.Y.: McGraw-Hill, 1968, Ch. 2-4).

42. Tupholme GE. Generation of acoustic pulses by baffled plane pistons, *Mathematika 16,* 209-224 (1969).

43. Stepanishen PR. The time-dependent force and radiation impedance on a piston in a rigid infinite planar baffle, *J Acoust Soc Amer 49,* 841-849 (1971).

44. Harris GR. Review of transient field theory for a baffled planar piston, *J Acoust Soc Amer 70,* 1-20 (1981).

45. Jensen JA, Svendsen NB. Calculation of pressure fields from arbitrily shaped, apodized, and excited ultrasound transdcuers, *IEEE Trans Ultrason Ferroelec Freq Contr 39* (1992).

46. Jensen JA. A new calculation procedure for spatial impulse responses in ultrasound, *J Acoust Soc Amer 105,* 3266-3274 (1999).

47. John F. *Partial Differential Equations* (New York: Springer-Verlag, 1982).

48. Bracewell R. *The Fourier Transform and its Applications* (New York: McGraw-Hill. 1965).

49. Brigham EO. *The Fast Fourier Transform* (Englewood Cliffs, NJ: Prentice-Hall, 1974).

50. Oppenheim AV, Schafer RW. *Digital Signal Processing* (Englewood Cliffs, NJ: Prentice-Hall, 1975, ch. 5).

51. Kino GS. *Acoustic Waves: Devices, Imaging, and Analog Signal Processing* (Englewood Cliffs, NJ: Prentice-Hall, 1987, ch. 3).

52. Burckhardt CB, Hoffmann H, Grandchamp PA. Ultrasound Axicon: a device for focusing over a large depth, *J Acoust Soc Amer 54,* 1628-1630 (1973).

53. Foster FS, Patterson MS, Arditi M, Hunt JW. The conical scanner: a two transducer ultrasound scatter imaging technique, *Ultrasonic Imaging 3,* 62-82 (1981).

ULTRASONIC IMAGING

An International Journal

ISSN 0161-7346

Volume 27, Number 3, July 2005

DYNAMEDIA, INC.

Silver Spring, MD

Volume 27, Number 4, October 2005

Ultrasonic Imaging
Volume 27, Number 4, October 2005

CONTENTS

ULTRASONIC IMAGING

Pages 201-272